# Perspectives of parameter and state estimation in paleoclimatology

André Paul*and Martin Losch†

October 25, 2011

**Abstract**

Past climates provide a means for evaluating the response of the climate system to large perturbations. Our ultimate goal is to constrain climate models rigorously by paleoclimate data. For illustration, we used a conceptual climate model (a classical energy balance model) and applied the so-called "adjoint method" to minimize the misfit between our model and sea-surface temperature data for the Last Glacial Maximum (LGM, between 19,000-23,000 years before present). The "adjoint model" (derivative code) was generated by an "adjoint compiler". We optimized parameters controlling the thermal diffusion and the sensitivity of the outgoing longwave radiation to changes in the zonal-mean surface temperature and the atmospheric $CO_2$ concentration. As a result, we estimated that an equilibrium climate sensitivity between 2.2 °C and 2.5 °C was consistent with the reconstructed glacial cooling, and we were able to infer structural deficits of the simple model where the fit to current observations and paleo data was not successful.

## 1 Introduction

Milankovitch is mainly renowned for his computation of the incoming solar radiation (insolation) at the top of the atmosphere over the past 600,000 years for different latitudes and seasons (Milankovitch, 1920, 1930, 1941). Yet he also formulated one of the early "climate models": He used the energy balance as implied by the planetary albedo and the outgoing longwave radiation according to the Stefan-Boltzmann law to infer the solar temperatures on the Earth's surface if it were covered uniformly by land and the atmosphere and ocean were at rest (Milankovitch, 1920, pp. 200); he compared these solar temperatures to then-current observations by Hann (1915). Furthermore, he computed the fluctuations in the extent of the polar ice caps in response to the fluctuations in insolation, even taking into account the feedback of the increasing albedo and surface height of a growing ice cap on temperature (Milankovitch, 1941). Finally,

*MARUM - Center for Marine Environmental Sciences and Department of Geosciences, University of Bremen, PO Box 33 04 40, D-28334 Bremen, Germany; E-mail: apaul@marum.de

†Alfred Wegener Institute for Polar and Marine Research, Bussestrasse 24, D-27570 Bremerhaven, Germany; E-mail: martin.losch@awi.de

he related the predictions of his climate model to geological data published by Penck and Brückner (1909). Thus he could associate four minima of his famous radiation curves, expressed in terms of equivalent latitudes, with the European ice ages as they were known at the time (for more detailed accounts of Milankovitch's achievements, see Berger, 1988; Petrović, 2002; Loutre, 2003; Grubić, 2006).

Formulating a climate model, then solving it either analytically or numerically, calibrating it against current observations, applying it to past conditions and relating its predictions to geological data – this is the traditional or "forward" method of paleoclimate modeling that Milankovitch pioneered in the first half of the last century. So-called "state-of-the-art" climate models are much more complex than their early predecessors and require long computing times, so that often only a few simulations are carried out. If at all feasible, models are "tuned" by adjusting individual parameters (or a parameterization) and repeating simulations in an *ad hoc* iteration (cf. Fig. 1a).

Today's comprehensive climate models and wealth of available observations, however, warrant to overcome such a crude tuning procedure and use the data to systematically fit models to data – that is, to (1) optimize model parameter values by "parameter estimation" or "calibration", (2) test the model for consistency with independent datasets, if available and (3) use the calibrated model for predictions.

The proper calibration of a climate model, as opposed to simply tuning it, implies the formulation of a statistical model that links evaluations of the climate model, the model parameters and observations on climate (Rougier, 2008). The focus is either on time evolution or the steady state of the climate system. While the "Bayesian" approach deals with probability density functions, the "maximum likelihood" approach aims for a point estimate of the model parameters.

Typically, the departure of the model from the data (the model-data misfit) is measured by an objective or cost function. In formulating this function, the uncertainties of both the model and the data can be considered. The cost function is usually a quadratic function of model-data differences weighted by their prior error estimates, but it can also include constraints that represent other prior knowledge of the climate.

An explicit cost function may be combined with the forward method to quantify the purpose of the numerical model (Wunsch, 1996). Then the parameter estimation may be carried out simultaneously with a "state estimation" and yield an estimate of, for example, the state of the ocean or atmosphere. One of the first examples of combined parameter and state estimation in the context of sparse paleoclimate data is given by Paul and Schäfer-Neth (2005).

It is desirable to automate the manual search for the optimum fit by using an algorithmic process. Available methods include statistical methods (e.g., Monte Carlo and Greene's function methods, ensemble Kalman and particle filter methods – Fig. 1b) as well as variational techniques and sequential filtering (e.g., the adjoint method or a Kalman filter/smoother – Fig. 2). The variational methods and the Kalman filter and smoother are especially suited to take into account the uncertainties associated with both model and data (e.g., Kasibhatla et al., 2000).

In the following, we use the adjoint method (e.g., Le Dimet and Talagrand, 1986;

Errico, 1997) to estimate the model parameters based on observations of the steady-state seasonal cycle. For a more probabilistic (Bayesian) approach, we refer to Edwards et al. (2007), Annan and Hargreaves (2007) and Holden et al. (2010).

The adjoint method requires an adjoint or dual model of a given forward model. Often this adjoint model is obtained through the application of an "adjoint compiler", a software tool that takes the computer source code of the forward model as input, applies the rules of automatic differentiation and yields the source code of the "adjoint model" (derivative code) as output (Giering, 2000; Rayner et al., 2000; Griewank and Walther, 2008).

The minimum of the cost function is searched for by varying control variables such as initial conditions, boundary conditions or internal parameters. The adjoint model computes the gradient of the cost function with respect to these control variables and provides the information required by a gradient descent algorithm. The gradients themselves contain valuable information on the sensitivity of the system to perturbations in the control variables.

We present a simple "textbook example" to illustrate the calibration of a climate model with the adjoint method (i.e., computing exact derivatives using automatic differentiation) in a paleoclimate context. To this end, we implemented a classical one-dimensional energy balance-climate model with seasonal insolation forcing. The corresponding adjoint model was generated by the "Tangent linear and Adjoint Model Compiler" (TAMC, `http://autodiff.com/tamc/`). We defined a seasonal cost function that allowed us to use paleo-sea surface temperature data to constrain the model[1].

# 2 Material and Methods

## 2.1 Energy balance-climate model

Our energy balance model is a conceptual climate model based on the difference between absorbed solar radiation $Q_{\mathrm{abs}}$ and outgoing longwave radiation $F_{\infty}^{\uparrow}$ at the top of the atmosphere (TOA) on the one hand, and the divergence of the horizontal heat transport $\Delta F_{\mathrm{ao}}$ on the other hand (see Hartmann, 1994, p. 237). In its one-dimensional version, the only coordinate variables are latitude $\phi$ and time $t$. Climate is expressed in terms of just one model variable, the zonally-averaged surface temperature $T_{\mathrm{s}}$:

$$\overline{C}_{\mathrm{ao}} \frac{\partial}{\partial t} T_{\mathrm{s}}(x,t) = R_{\mathrm{TOA}}(x,t,T_{\mathrm{s}}) - \Delta F_{\mathrm{ao}}(x,t,T_{\mathrm{s}}) \;, \tag{1}$$

where $x = \sin\phi$, $\overline{C}_{\mathrm{ao}} = c_{\mathrm{p}}\,\rho_{\mathrm{w}}\,H_{\mathrm{o}}$ is the effective heat capacity of the atmosphere-ocean system (with $c_{\mathrm{p}}$ and $\rho_{\mathrm{w}}$ being the specific heat and density of water and $H_{\mathrm{o}}$ the ocean mixed-layer depth) and $R_{\mathrm{TOA}}$ the net incoming radiation at the top of the atmosphere, which is expressed as the difference between absorbed solar radiation $Q_{\mathrm{abs}}(x,t,T_{\mathrm{s}})$ and

[1] The code of the one-dimensional energy balance-climate model and its adjoint `Ebm1D` is available upon request from apaul@marum.de

outgoing longwave radiation $F^{\uparrow}_{\infty}(x, T_\mathrm{s})$:

$$R_\mathrm{TOA}(x, t, T_\mathrm{s}) = Q_\mathrm{abs}(x, t, T_\mathrm{s}) - F^{\uparrow}_{\infty}(x, T_\mathrm{s}) \; . \tag{2}$$

The absorbed solar radiation is the product of one-fourth of the solar constant, $S_0/4$, a function that describes the distribution of insolation with latitude and time of year, $s(x, t)$ – cf. Berger (1978), and the absorptivity for solar radiation, $a_\mathrm{p}(x, T_\mathrm{s})$:

$$Q_\mathrm{abs}(x, t, T_\mathrm{s}) = \frac{S_0}{4} \, s(x, t) \, a_\mathrm{p}(x, T_\mathrm{s}) \; . \tag{3}$$

The absorptivity is related to the planetary albedo $\alpha_\mathrm{p}(x, T_\mathrm{s})$ through the relationship $a_\mathrm{p}(x, T_\mathrm{s}) = 1 - \alpha_\mathrm{p}(x, T_\mathrm{s})$. In our case, the absorptivity is given by:

$$a_\mathrm{p}(x, x_\mathrm{i}) = \begin{cases} a_0 + a_2 P_2(x) \; , & T_\mathrm{s} > -10°\mathrm{C} \; , |x| < |x_\mathrm{ice}| \; , \\ b_0 \; , & T_\mathrm{s} < -10°\mathrm{C} \; , |x| > |x_\mathrm{ice}| \; , \end{cases} \tag{4}$$

where $a_0$, $a_2$ and $b_0$ are constant coefficients, $P_2$ refers to the Legendre polynomial of second order in $x$,

$$P_2(x) = \frac{1}{2} \left( 3x^2 - 1 \right) \; , \tag{5}$$

and $x_\mathrm{ice}$ is the position of the point where the temperature equals $-10°\mathrm{C}$. This point is called the iceline.

The outgoing longwave radiation is parameterized as a linear function of the surface temperature and the logarithm of the ratio of the actual value of the atmospheric $CO_2$ concentration $[CO_2]$ to a reference value $[CO_2]_\mathrm{ref}$:

$$F^{\uparrow}_{\infty}(x, T_\mathrm{s}) = A + B \, T_\mathrm{s} - \Delta Q_{2\times \mathrm{CO_2}} \; \log \left( [\mathrm{CO_2}] / [\mathrm{CO_2}]_\mathrm{ref} \right) / \log 2 \; , \tag{6}$$

where $A$, $B$ and $\Delta Q_{2\times \mathrm{CO_2}}$ are constant coefficients; in particular, $B$ describes the efficiency of longwave radiative cooling and $\Delta Q_{2\times \mathrm{CO_2}}$ is the radiative forcing equivalent to a doubling of the atmospheric $CO_2$ concentration (cf. Myhre et al., 1998). The outgoing longwave radiation increases only linearly with temperature, rather than as the fourth power of temperature as indicated by the Stefan-Boltzmann law. This is a simple way to account for the effect of the water vapor feedback when the relative humidity is assumed to be constant (Hartmann, 1994, p. 233) .

Meridional (north-south) heat transport is treated as a diffusive process, driven by latitudinal temperature gradients, an approach considered to be valid at horizontal scales of about 1500 km and larger and time scales of 6 months and longer (Lorenz, 1979):

$$\Delta F_\mathrm{ao} = \frac{1}{a} \frac{\partial}{\partial x} \left( \sqrt{1 - x^2} \; F_\mathrm{ao} \right) \tag{7}$$

and

$$F_\mathrm{ao} = -\overline{C}_\mathrm{ao} K_\mathrm{ao}(x) \frac{\sqrt{1 - x^2}}{a} \frac{\partial T_\mathrm{s}}{\partial x} \; , \tag{8}$$

where $a$ is the mean radius of Earth and the thermal diffusion coefficient $K_{\mathrm{ao}}$ is given by:

$$K_{\mathrm{ao}}(x) = K_0 \left(1 + K_2\, x^2 + K_4\, x^4\right) \ . \tag{9}$$

Here $K_0$, $K_2$ and $K_4$ are constant coefficients.

The values of all model parameters are listed in Table 1. The model equations are discretized using centered differences in space and forward differences in time. The meridional grid is staggered. The thermal diffusion coefficient is defined at $U$ grid points that are half-way between the temperature or $T$ grid points.

## 2.2 Data

The target for our present-day simulation (Experiment PD1) is the surface air temperature from the NCEP/NCAR reanalysis data [Kalnay et al. (1996) – see Fig. 3].

As an example target for our paleo-simulations (Experiments LGM1 and LGM2), we chose the sea-surface temperature anomaly between the Last Glacial Maximum (LGM – 19,000-23,000 years before present) and present day as reconstructed by the GLAMAP 2000 project (Sarnthein et al., 2003). In the context of a one-dimensional energy balance model, we prefer it over the more recent MARGO reconstruction (Kucera et al., 2005; MARGO Project Members, 2009), because the objective mapping by Schäfer-Neth and Paul (2004) of the sparse proxy data at the ocean sediment core locations allows for consistent zonal averaging. The annual mean and February and August monthly means of the reconstructed SST anomaly are shown – along with the model results – in Figs 5 and 6.

## 2.3 Cost function

The cost function (also called the objective or mismatch function) used for our present-day experiments is defined by:

$$J = \sum \frac{\left(T_{\mathrm{s}}^{\mathrm{Feb,\,mod}} - T_{\mathrm{s}}^{\mathrm{Feb,\,obs}}\right)^2}{\sigma_{T_{\mathrm{s}}}^2} + \sum \frac{\left(T_{\mathrm{s}}^{\mathrm{Aug,\,mod}} - T_{\mathrm{s}}^{\mathrm{Aug,\,obs}}\right)^2}{\sigma_{T_{\mathrm{s}}}^2} \ . \tag{10}$$

Here "obs" and "mod" refer to observed and modeled, and $\sigma_{T_{\mathrm{s}}} = 1\,^{\circ}\mathrm{C}$ in the denominator refers to the error in surface temperature. The sums extend over all latitude zones of the one-dimensional energy balance-climate model that contain data and are weighted by the respective surface area.

Correspondingly, the cost function used for our LGM experiments is defined by:

$$J = \sum \frac{\left(\Delta T_{\mathrm{s}}^{\mathrm{Feb,\,mod}} - \Delta T_{\mathrm{s}}^{\mathrm{Feb,\,rec}}\right)^2}{\sigma_{\Delta T_{\mathrm{s}}}^2} + \sum \frac{\left(\Delta T_{\mathrm{s}}^{\mathrm{Aug,\,mod}} - \Delta T_{\mathrm{s}}^{\mathrm{Aug,\,rec}}\right)^2}{\sigma_{\Delta T_{\mathrm{s}}}^2} \ , \tag{11}$$

where "rec" refers to reconstructed and $\sigma_{\Delta T_{\mathrm{s}}} = 1\,^{\circ}\mathrm{C}$.

In computing the cost function, we use the angular definition of seasons proposed by Joussaume and Braconnot (1997) (see Table 2).

Table 1: First-guess values of model parameters. In case of the selected control variables, they were subject to change during the optimization process. For the value of the solar constant, we followed the protocol of the Paleoclimate Modeling Intercomparison Project (PMIP) 1, see Joussaume and Taylor (1995).

| Symbol | Value | Units | Description | Reference |
|---|---|---|---|---|
| $a$ | $6.371 \times 10^6$ | m | mean radius of Earth | |
| $\rho_\mathrm{w}$ | 1000 | kg m$^{-3}$ | density of pure water at 0 °C | |
| $c_\mathrm{p}$ | 4218 | J kg$^{-1}$ K$^{-1}$ | specific heat of liquid water at 0 °C | |
| $H_\mathrm{o}$ | 70 | m | ocean mixed-layer depth | Hartmann (1994, p. 84) |
| $S_0$ | 1365 | W m$^{-2}$ | present-day solar constant | Joussaume and Taylor (1995) |
| *Linearized longwave radiation:* | | | | |
| $A$ | 205.0 | W m$^{-2}$ | constant term | Hartmann and Short (1979, set 2) |
| $B$ | 2.23 | W m$^{-2}$ K$^{-1}$ | efficiency of longwave radiative cooling | Hartmann and Short (1979, set 2) |
| $\Delta Q_{2\times\mathrm{CO_2}}$ | 4.0 | W m$^{-2}$ | 2×$CO_2$ radiative forcing | Hartmann (1994, p. 232) |
| $[\mathrm{CO_2}]_\mathrm{ref}$ | 345 | ppmv | reference atmospheric $CO_2$ concentration | Joussaume and Taylor (1995) |
| $[\mathrm{CO_2}]$ | 345 or 200 | ppmv | actual atmospheric $CO_2$ concentration | |
| *Albedo coefficients:* | | | | |
| $b_0$ | 0.38 | | icecovered absorptiviity | Hartmann and Short (1979, set 2) |
| $a_0$ | 0.697 | | coefficient in ice-free absorptiviity | Hartmann and Short (1979, set 2) |
| $a_2$ | -0.175 | | coefficient in ice-free absorptiviity | Hartmann and Short (1979, set 2) |
| $T_\mathrm{ice}$ | -10 | °C | critical temperature for ice formation | Hartmann (1994, p. 238) |
| *Diffusion coefficients:* | | | | |
| $K_0$ | $1.5 \times 10^5$ | m$^2$ s$^{-1}$ | constant factor | |
| $K_2$ | -1.33 | | second-order coefficient | North et al. (1983) |
| $K_4$ | 0.67 | | fourth-order coefficient | North et al. (1983) |

| Date | True longitude | Day number 1950 AD orbit | 21 ka BP orbit |
|---|---|---|---|
| Vernal equinox, 21 March, 12:00 | 0° | 80.0 | 80.0 |
| 1 February, 0:00 | -48.78° | 31.50 | 31.91 |
| 28 February, 24:00 | -20.48° | 59.50 | 59.68 |
| 1 August, 0:00 | 127.97° | 212.50 | 212.27 |
| 31 August, 24:00 | 157.80° | 243.50 | 243.52 |

Table 2: Angular definition of seasons. The vernal equinox is taken as a reference. Correspondingly, perihelion occurs at day number 2.85 (1950 AD orbit) and 15.51 (21 ka BP orbit), respectively (Berger, 1978).

### 2.4 Optimization algorithm

For minimization of the cost function, we used a variable memory quasi-Newton algorithm as implemented in M1QN3 by Gilbert and Lemaréchal (1989). This algorithm computes a local approximation of the inverse Hessian matrix based on the gradient of the cost function and generally converges faster than conventional conjugate gradient methods (see also `http://www-rocq.inria.fr/~gilbert/modulopt/optimization-routines/m1qn3/m1qn3.html`).

As a stopping criterion, we required a relative precision on the norm of the gradient of the cost function of $10^{-4}$.

### 2.5 Experimental setup

The meridional resolution was set to 10°. All experiments were integrated for 100 years using a time step of one day. The last 10 years of each experiment were used for calculating the cost function and analyzing the model results.

Table 3 lists the seven base experiments that were carried out with the one-dimensional energy balance-climate model. In the case of Experiment PD0, we used the first-guess values for all model parameters without any optimization, while in Experiment PD1 (the "control simulation" for the present-day climate), we used the parameters $H_o$ for the ocean mixed-layer depth, $K_0$, $K_2$ and $K_4$ of the heat diffusion coefficient and $A$ of the outgoing longwave radiation as control variables that were adjusted using the adjoint method.

In Experiment LGM1, the optimized parameter values of Experiment PD1 were held fixed. The only control variable was the parameter $\Delta Q_{2\times CO_2}$ affecting the radiative forcing associated with the change of the atmospheric $CO_2$ concentration from 345 ppmv to 200 ppmv. In Experiment LGM2, we added the parameters $K_0$, $K_2$ and $K_4$ of the heat diffusion coefficient to the control variables.

For Experiments LGM1 and LGM2, we followed the PMIP1 protocol (see `http://pmip.lsce.ipsl.fr/newsletters/newsletter02.html`) and used 200 ppmv as atmospheric $CO_2$ concentration.

In Experiments 2xCO2_1, 2xCO2_2 and 2xCO2_3, we studied the effect of doubling the atmospheric $CO_2$ concentration from 345 ppmv to 690 ppmv on the equilibrium conditions in our one-dimensional energy balance-climate model. Again, we used the optimized parameter values of Experiment PD1. The parameter $\Delta Q_{2\times CO_2}$ was set to the first-guess value, the value obtained from Experiment LGM1 and the value obtained from Experiment LGM2, respectively (Table 3).

Table 4 lists eight additional experiments that were designed to study the sensitivity of the optimal solution for Experiment LGM2 to the initial values of the control variables. In Experiments LGM2_1 and LGM2_2, the initial value of $\Delta Q_{2\times CO_2}$ was varied. In Experiments LGM2_3 and LGM2_4, the initial value of $K_0$ was varied. Experiments LGM2_5 to LGM2_8 allowed for combinations of changes in $\Delta Q_{2\times CO_2}$ and $K_0$.

| | | Experiment | | | | | | |
|---|---|---|---|---|---|---|---|---|
| Parameter | Units | PD0 | PD1 | LGM1 | LGM2 | 2xCO2_1 | 2xCO2_2 | 2xCO2_3 |
| $n$ | | – | 5 | 1 | 4 | – | – | – |
| $[CO_2]$ | ppmv | 345 | 345 | 200 | 200 | 690 | 690 | 690 |
| $H_o$ | m | 70 | *27.4* | 27.4 | 27.4 | 27.4 | 27.4 | 27.4 |
| $A$ | W m$^{-2}$ | 205.0 | *209.6* | 209.6 | 209.6 | 209.6 | 209.6 | 209.6 |
| $B$ | W m$^{-2}$ K$^{-1}$ | 2.23 | 2.23 | 2.23 | 2.23 | 2.23 | 2.23 | 2.23 |
| $K_0$ | $10^5$ m$^2$ s$^{-1}$ | 1.5 | *3.8* | 3.8 | *3.3* | 3.8 | 3.8 | 3.8 |
| $K_2$ | | -1.33 | *-0.64* | -0.64 | *-0.53* | -0.64 | -0.64 | -0.64 |
| $K_4$ | | 0.67 | *-0.32* | -0.32 | *-0.36* | -0.32 | -0.32 | -0.32 |
| $\Delta Q_{2\times CO_2}$ | W m$^{-2}$ | – | – | *4.97* | *4.39* | 4.0 | 4.97 | 4.39 |
| $J$ | | 28.42 | 13.27 | 1.34 | 0.76 | – | – | – |
| $N_{\text{iterations}}$ | | – | 190 | 3 | 39 | – | – | – |
| $N_{\text{simulations}}$ | | – | 236 | 4 | 47 | – | – | – |

Table 3: Experimental setup. The number control variables is denoted by $n$. The values of the control variables after optimization are given in italics. The number of iterations is given by $N_{\text{iterations}}$, while the total number of simulations perfomed by the optimization algorithm is referred to as $N_{\text{simulations}}$.

# 3 Results

Table 5 summarizes the results of the four experiments in terms of the planetary albedo, the global mean temperature and the latitude of the ice boundary. There is almost no change in the annually and globally averaged planetary albedo $\overline{\alpha_p}^{\text{ann}}$ between the different experiments. With all model parameters set to their first-guess values in Experiment PD0, the global mean temperature $\overline{T_s}$ is above 16 °C during all seasons. Optimizing the model parameters in Experiment PD1 led to the reduction of the cost function (Eq. 10) by one-half and required 190 iterations (Table 3). The ocean mixed-layer depth $H_o$ was reduced to 27.4 m. At the same time, $\overline{T_s}^{\text{ann}}$ decreased by 2.4 °C and the icelines $\overline{\phi_{\text{ice}}^{\text{S,N}}}^{\text{ann}}$

| Parameter | Units | Experiment | | | | | | | | |
|---|---|---|---|---|---|---|---|---|---|---|
| | | LGM2 | LGM2_1 | LGM2_2 | LGM2_3 | LGM2_4 | LGM2_5 | LGM2_6 | LGM2_7 | LGM2_8 |
| | | *Initial values of control variables* | | | | | | | | |
| $K_0$ | $10^5$ m$^2$ s$^{-1}$ | 3.7646 | 3.7646 | 3.7646 | *0.3900* | *8.9000* | *1.4000* | *8.9000* | *0.8400* | *8.9000* |
| $K_2$ | | -0.6408 | -0.6408 | -0.6408 | -0.6408 | -0.6408 | -0.6408 | -0.6408 | -0.6408 | -0.6408 |
| $K_4$ | | -0.3239 | -0.3239 | -0.3239 | -0.3239 | -0.3239 | -0.3239 | -0.3239 | -0.3239 | -0.3239 |
| $\Delta Q_{2\times CO_2}$ | W m$^{-2}$ | 4.0000 | *1.1000* | *4.7000* | 4.0000 | 4.0000 | *1.1000* | *1.1000* | *4.7000* | *4.7000* |
| | | *Optimized values of control variables* | | | | | | | | |
| $K_0$ | $10^5$ m$^2$ s$^{-1}$ | 3.2894 | 3.2933 | 3.2918 | 3.3543 | 3.333 | 3.3210 | 3.2840 | 3.2037 | 3.3358 |
| $K_2$ | | -0.5347 | -0.5386 | -0.5371 | -0.5971 | -0.5788 | -0.5672 | -0.5287 | -0.4446 | -0.5820 |
| $K_4$ | | -0.3578 | -0.3536 | -0.3552 | -0.2913 | -0.3102 | -0.3225 | -0.3643 | -0.4548 | -0.3066 |
| $\Delta Q_{2\times CO_2}$ | W m$^{-2}$ | 4.3858 | 4.3839 | 4.3844 | 4.3483 | 4.3663 | 4.3719 | 4.391 | 4.4275 | 4.3626 |
| $J$ | | 0.7620 | 0.7620 | 0.7620 | 0.7636 | 0.7627 | 0.7624 | 0.7621 | 0.7655 | 0.7629 |

Table 4: Additional experiments on the sensitivity of the optimal solution. *Top:* Initial values of the control variables. Values of the control variables that are different from their first-guess values are given in italics. Experiment LGM2 is the original simulation using the first-guess values for all $n = 4$ control variables. *Bottom:* Values of the control variables and the cost function after optimization.

moved equatorward by 2°–3° in latitude. Applying the adjoint method to the LGM climate conditions in Experiment LGM1 led to a global mean glacial cooling of 2 °C and a growth of the polar ice caps by about 2° in latitude. Adding the parameters in the heat diffusion coefficient to the control variables in Experiment LGM2 hardly affected the global mean temperature, but caused the icelines to shift further equatorward by nearly 1° in latitude. The radiative forcing parameter $\Delta Q_{2\times CO_2}$ (see Eq. 6) was increased by 24% in Experiment LGM1 and 10% in Experiment LGM2, compared to the first-guess value of 4 W $m^{-2}$ (Table 1). We speculate that this increase partly compensated for other positive feedbacks that are missing from the model, such as the full water-vapor feedback.

Fig. 3 shows that in Experiment PD0 the largest differences in the simulated and the observed temperature occurred near the South Pole and in the high northern latitudes. In the south the model temperatures were generally higher than the observations. In the north, by contrast, the model climate was warmer than observed during winter and colder during summer. Fig. 4 indicates for Experiment PD1 a generally closer fit to the observations than for Experiment PD0, except near the poles.

With $\Delta Q_{2\times CO_2}$ as the only control variable in Experiment LGM1, the glacial cooling as a function of latitude was nearly flat, with only a small polar amplification, as can be seen from Fig. 5. Allowing for changes in the thermal diffusion coefficient in Experiment LGM2, the polar amplification became more prominent (Figs 6 and 7).

Comparing Experiments PD1 (Fig. 4) and LGM2 (Fig. 6), the meridional heat transport generally decreased during Northern Hemisphere winter (February) and increased during Northern Hemisphere summer (August), except for the high latitudes (Fig. 8). In the high latitudes, the meridional heat transport decreased in the south and increased in the north during the entire year.

With respect to Experiment PD1, Experiments 2xCO2_1, 2xCO2_2 and 2xCO2_3 led to an increase of the global mean temperature by 2.0 °C, 2.5 °C and 2.2 °C, respectively (Table 5). At the same time, the icelines in both hemisphere moved poleward by 1.95°, 2.4° and 2.13° in latitude, respectively.

Regarding the sensitivity of the optimal solution for Experiment LGM2 to the initial values of the control variables, the optimization converged for a wide range of initial values of $\Delta Q_{2\times CO_2}$ to the same minimum of the cost function with similar values of the optimized control variables (cf. Experiments LGM2_1 and LGM2_2, Table 4). It also converged outside of this range, but not to the required relative precision on the norm of the gradient of the cost function of $10^{-4}$. Similarly, the optimization converged for a wide range of initial values of $K_0$ to nearly the same minimum of the cost function (cf. Experiments LGM2_3 and LGM2_4). Outside of this range, however, it did not converge. Finally, the results of Experiments LGM2_5 to LGM2_8 indicate the common ranges of these two control variables for which convergence was still possible.

| | | Experiment | | | | | | |
|---|---|---|---|---|---|---|---|---|
| Variable | Units | PD0 | PD1 | LGM1 | LGM2 | 2xCO2_1 | 2xCO2_2 | 2xCO2_3 |
| $\overline{\alpha_\mathrm{p}}^{\mathrm{ann}}$ | | 0.31 | 0.32 | 0.32 | 0.32 | 0.32 | 0.32 | 0.32 |
| $\overline{T_\mathrm{s}}^{\mathrm{ann}}$ | °C | 16.21 | 13.81 | 11.81 | 11.88 | 15.84 | 16.33 | 16.04 |
| $\overline{T_\mathrm{s}}^{\mathrm{Feb}}$ | °C | 16.29 | 14.03 | 12.00 | 12.07 | 16.06 | 16.55 | 16.26 |
| $\overline{T_\mathrm{s}}^{\mathrm{Aug}}$ | °C | 16.10 | 13.51 | 11.55 | 11.62 | 15.55 | 16.03 | 15.74 |
| $\overline{\phi_\mathrm{ice}^\mathrm{S}}^{\mathrm{ann}}$ | | -68.69° | -65.42° | -63.31° | -62.56° | -67.37° | -67.83° | -67.56° |
| $\overline{\phi_\mathrm{ice}^\mathrm{N}}^{\mathrm{ann}}$ | | 67.84° | 65.49° | 63.39° | 62.64° | 67.44° | 67.90° | 67.62° |

Table 5: Selected experimental results: Annual and global average of the planetary albedo $\overline{\alpha_\mathrm{p}}^{\mathrm{ann}}$, annual, February and August averages of the global mean temperature $\overline{T_\mathrm{s}}^{\mathrm{ann}}$, $\overline{T_\mathrm{s}}^{\mathrm{Feb}}$ and $\overline{T_\mathrm{s}}^{\mathrm{Aug}}$ and annual-mean latitude of the ice boundary in the Southern and Northern Hemispheres $\overline{\phi_\mathrm{ice}^\mathrm{S}}^{\mathrm{ann}}$ and $\overline{\phi_\mathrm{ice}^\mathrm{N}}^{\mathrm{ann}}$.

# 4 Discussion

We illustrated how the so-called adjoint method could be used to adjust the parameters of a simple climate model so that the model predictions were consistent with either modern surface temperature observations (Fig. 4) or reconstructed LGM sea-surface temperature anomalies (Fig. 5). The model-data fit improved further (Fig. 6) by additionally adjusting the thermal diffusion coefficient (Fig. 7), although at the cost of implausibly large positive temperature anomalies very near the poles.

The remaining model discrepancy points to a structural error of our simple climate model. As opposed to a parametric error, this error cannot be removed by adjusting the parameter values; it is rather an error in the functional form of the model equations or their numerical implementation (that is, in their discretization in space and time).

Correspondingly, even after optimizing the parameter values, our energy balance-climate model does not simulate a realistic present-day climate. For example, the simulated latitude of the ice boundary in the Northern Hemisphere in Experiments PD0 (≈67.8° N) and PD1 (≈66.5° N) is considerably lower than the approximate current position of the ice edge (≈71.8° N, e.g., Jentsch, 1987). This is likely due to an overly simplistic representation of the ice-albedo feedback. In this respect, the value of the critical temperature for the formation of ice $T_\mathrm{ice} = -10$ °C is derived from the observed annual-mean temperature at which surface ice cover persists throughout the year (Hartmann, 1994, p. 238). A higher value (around 0 °C) may be more appropriate to parameterize the seasonal formation of snow and ice but by itself lead to an even lower latitude of the ice boundary.

The optimized value of the ocean mixed-layer depth of 27.4 m is smaller than the value of 50 m–70 m that is often taken as the depth of the top layer of the ocean that interacts with the the atmosphere on a timescale of a year (Hartmann, 1994, p. 84), probably because we ignored the land cover with a much smaller thermal capacity. A

slightly more realistic climate model would include a variable land fraction as a function of latitude.

Other contributions to the structural error include the lack of: zonal (east-west) and vertical resolution, a diurnal cycle, clouds, a realistic representation of the greenhouse effect, light scattering within the atmosphere and a separate treatment of the atmosphere, ocean and land surface components of the climate system and their interactions.

Furthermore, our simulations of the LGM climate were possibly biased towards a low value of the radiative forcing parameter $\Delta Q_{2\times CO_2}$, because the GLAMAP 2000 project (Sarnthein et al., 2003) may slightly underestimate the glacial cooling as compared to more recent reconstructions (e.g., MARGO Project Members, 2009). Consequently, the optimal values of $\Delta Q_{2\times CO_2}$ (5.0 W m$^{-2}$ in Experiment LGM1 and 4.4 W m$^{-2}$ in Experiment LGM2, Table 3) correspond to an equilibrium climate sensitivity (an equilibrium change in global mean temperature for a sustained doubling of the atmospheric $CO_2$ concentration) between 2.2 °C and 2.5 °C (Table 5), which is towards the lower end of the range between 1.2 °C and 4.3 °C estimated from an ensemble of simulations of the LGM climate (Schneider von Deimling et al., 2006) and the range between 2.0 °C and 4.5 °C in the current IPCC assessment (Meehl et al., 2007).

The question of how to take into account the structural error (possibly by expert judgment or multi-model ensembles, cf. Rougier, 2008) is crucial to the problem of model calibration. In a maximum-likelihood approach as taken by the adjoint method, and assuming a Gaussian probability density distribution, the covariance matrix of the model discrepancy and the covariance matrix of the observational error ($\sigma_{T_s}$ in Eqs. 10 and 11) would both determine the cost and hence the results. However, the two covariance matrices could be very different from each other. What is more, it may even be questioned that the structural error can be properly described by a Gaussian probability density distribution.

We note that our definitions of the present-day and LGM cost functions in Eqs. 10 and 11 do not contain a term related to the structural error – nor do they include a so-called "background term", which in our case would penalize deviations between the optimal and the first-guess values of the control variables. Such a term is necessary whenever the system of model equations is underdetermined (i.e. if the information contained in the observations is insufficient to guarantee a unique optimal solution). In our case, however, we used observations in every latitude zone of the model; thus the system was likely to be "well-observed". Indeed, by performing additional experiments using different initial values for the optimization, we confirmed that our optimal solution for the LGM was unique for a broad range of the control variables $K_0$ and $\Delta Q_{2\times CO_2}$, because the optimized values of the control variables were not significantly different from each other (Table 4). Significant differences would have indicated a sensitive dependence on the first-guess values of the control variables and thus a non-uniqueness of the optimized solution.

Since a sensitive dependence on initial conditions is a characteristic of a nonlinear system, failure of convergence or convergence to a different local minimum of the cost function is to be expected outside of a given range of the optimal values of the control

variables. This ambiguity may be removed by including a background term into the cost function, i.e., by adding prior knowledge on the likely values of the control variables (see, e.g. Losch and Wunsch, 2003).

We point out that in our application of the adjoint method, the control variables only consisted of internal parameters in the underlying equations of the energy balance-climate model. An application that also includes initial conditions or boundary conditions is referred to as "data assimilation" rather than "parameter estimation" (e.g., Giering, 2000).

For many purposes, estimates of the errors of the optimal control variables are highly desirable. The adjoint method allows to estimate these errors, because for a Gaussian error distribution and in a linear approximation, the error covariance matrix of the control variables is the inverse Hessian matrix of the cost function $J$ at its minimum (Thacker, 1989; Giering, 2000). Indeed, the adjoint compiler TAMC provides a means for computing the uncertainties of a reasonably low number of control variables.

In comparison to the adjoint method, the Bayesian approach is designed from the outset to produce an entire multi-variate distribution of parameter values. It may help to select a suitable model by revealing two common symptoms of the structural error (Larson et al., 2008): underfitting (that is, when the structure of a model is not rich enough to capture the full variability in a dataset) and overfitting (when too many parameters are used to fit a limited dataset).

For example, it may happen that in the case of our energy balance-climate model no single set of parameter values (which are distinct within error bars) yields a good fit for all cases (pre-industrial and LGM), even though optimal parameter values can be obtained for each case separately. This may indicate underfitting in the sense that thermal diffusion is too simple to capture the full glacial-interglacial climate variability.

Regarding previous examples of state estimation in paleoclimatology, we point to the work of LeGrand and Wunsch (1995) and Winguth et al. (2000), who attempted to infer the ocean circulation during the LGM from reconstructed paleonutrient distributions.

# 5 Conclusions

Systematically fitting a "textbook example"-type climate model to paleoclimate data gave useful results: In a one-dimensional energy balance model, the glacial cooling reconstructed by the GLAMAP 2000 project (Sarnthein et al., 2003) was consistent with an equilibrium climate sensitivity for a doubling of the atmospheric $CO_2$ concentration between 2.2 °C and 2.5 °C. Besides calibrating our simple model to current observations and paleo data, we were able to infer contributions to its structural error where the fit was not successful.

While the adjoint method proved to be very efficient in optimizing the model parameter values, a Bayesian approach may in addition provide a natural framework to assess their uncertainty and help to avoid underfitting or overfitting the data.

These findings open up a wide field of applications to more complex climate models with many more parameters that can serve as control variables. Estimating model

parameters and states and identifying model problems for further model improvement are general goals of paleoclimate research.

We note that in spite of the simplicity of our model, we employed automatic differentiation (through the adjoint compiler TAMC). With complex models one will hardly succeed without such tools, and their development will be as important for this field as the evolution of numerical models.

## 6 Acknowledgments

AP expresses his sincere gratitude to the organizers of the "Milutin Milankovitch $130^{th}$ Anniversary Symposium" (Belgrade, 22-25 September 2009), who made this conference a very memorable and inspiring experience. We acknowledge the helpful discussions with Takasumi Kurahashi-Nakamura, as well as the instructive comments by Michel Crucifix and an anonymous reviewer. All graphs were drawn with the Generic Mapping Tools (Wessel and Smith, 1998). This research was funded by the DFG-Research Center/Center of Excellence MARUM – "The Ocean in the Earth System".

## References

Annan, J. D. and J. C. Hargreaves (2007). Efficient estimation and ensemble generation in climate modelling. *Philisophical Transactions of the Royal Society A 365*(1857), 2077–2088.

Berger, A. (1988). Milankovitch theory and climate. *Reviews of Geophysics 26*, 624–657.

Berger, A. L. (1978). Long term variations of daily insolation and Quaternary climatic changes. *Journal of the Atmospheric Sciences 35*(12), 2362–2367.

Edwards, T. L., M. Crucifix, and S. P. Harrison (2007). Using the past to constrain the future: how the palaeorecord can improve estimates of global warming. *Progress in Physical Geography 31*, 481–500, doi:10.1177/0309133307083295.

Errico, R. M. (1997). What is an adjoint model? *Bulletin of the American Meteorological Society 78*(11), 2577–2591.

Giering, R. (2000). Tangent linear and adjoint biogeochemical models. In P. Kasibhatla, M. Heimann, P. Rayner, N. Mahowald, R. G. Prinn, and D. E. Hartley (Eds.), *Inverse Methods in Global Biogeochemical Cycles*, Volume 114 of *Geophysical Monograph Series*, pp. 33–48. Washington, DC: AGU.

Gilbert, J. C. and C. Lemaréchal (1989). Some numerical experiments with variable storage quasi-Newton algoritms. *Mathematical Programming 45*, 407–435.

Griewank, A. and A. Walther (2008). *Evaluating Derivatives. Principles and Techniques of Algorithmic Differentiation* (2nd ed.), Volume 19 of *Frontiers in Applied Mathematics*. Philadelphia: SIAM.

Grubić, A. (2006). The astronomical theory of climatic changes of Milutin Milankovich. *Episodes 29*(3), 197–203.

Hann, J. v. (1915). *Lehrbuch der Meteorologie* (3rd ed.). Leipzig: C.H. Tauchnitz.

Hartmann, D. L. (1994). *Global Physical Climatology*. San Diego: Academic Press.

Hartmann, D. L. and D. A. Short (1979). On the role of zonal asymmetries in climate change. *Journal of the Atmospheric Sciences 36*, 519–528.

Holden, P. B., N. R. Edwards, K. I. C. Oliver, T. M. Lenton, and R. D. Wilkinson (2010). A probabilistic calibration of climate sensitivity and terrestrial carbon change in GENIE-1. *Climate Dynamics 35*, 785–806, doi:10.1007/s00382–009–0630–8.

Jentsch, V. (1987). Cloud-ice-vapor feedbacks in a global climate model. In C. Nicolis and G. Nicolis (Eds.), *Irreversible Phenomena and Dynamical Systems Analysis in Geosciences*, pp. 417–437. D. Reidel Publishing Company.

Joussaume, S. and P. Braconnot (1997). Sensitivity of paleoclimate simulation results to season definitions. *Journal of Geophysical Research 102*(D2), 1943–1956.

Joussaume, S. and K. Taylor (1995). Status of the Paleoclimate Modeling Intercomparison Project. In *Proceedings of the First International AMIP Scientific Conference, WCRP-92, Monterey, California, USA, 15-19 May 1995*, pp. 532 (425–430). Geneva, Switzerland: WMO/TD-No. 732.

Kalnay, E., M. Kanamitsu, R. Kistler, W. Collins, D. Deaven, L. Gandin, M. Iredell, S. Saha, G. White, J. Woolen, Y. Zhu, M. Chelliah, W. Ebisuzaki, W. Higgins, J. Janowiak, K. C. Mo, C. Ropelewski, L. A., R. Reynolds, and R. Jenne (1996). The NCEP/NCAR reanalysis project. *Bulletin of the American Meteorological Society 77*, 437–471.

Kasibhatla, P., M. Heimann, P. Rayner, N. Mahowald, R. G. Prinn, and D. E. Hartley (2000). *Inverse Methods in Global Biogeochemical Cycles*, Volume 114 of *Geophysical Monograph Series*. Washington, DC: AGU.

Kucera, M., A. Rosell-Melé, R. Schneider, C. Waelbroeck, and M. Weinelt (2005). Multiproxy approach for the reconstruction of the glacial ocean surface (margo). *Quaternary Science Reviews 24*, 813–819.

Larson, V. E., J. C. Golaz, J. Hansen, D. P. Schanen, and B. M. Griffin (2008). Diagnosing structural errors in climate model parameterizations. In *Extended Abstracts, 20th Conference on Climate Variability and Change, 88th Annual Meeting of the American Meteorological Society*. New Orleans, LA.

Le Dimet, F.-X. and O. Talagrand (1986). Variational algorithms for analysis and assimilation of meteorological observations: Theoretical aspects. *Tellus 38A*(2), 97–110.

LeGrand, P. and C. Wunsch (1995). Constraints from paleotracer data on the North Atlantic circulation during the last glacial maximum. *Paleoceanography 6*, 1011–1045.

Lorenz, E. N. (1979). Forced and free variations of weather and climate. *Journal of Atmospheric Sciences 36*(8), 1367–1376.

Losch, M. and C. Wunsch (2003). Bottom topography as a control parameter in an ocean circulation model. *Journal of Atmospheric and Oceanic Technology 20*(11), 1685–1696.

Loutre, M. F. (2003). Ice Ages (Milankovitch Theory). In J. R. Holton, J. A. Curry, and J. A. Pyle (Eds.), *Encyclopedia of Atmospheric Sciences*, pp. 995–1003. Elsevier.

MARGO Project Members (2009). Constraints on the magnitude and patterns of ocean cooling at the Last Glacial Maximum. *Nature Geoscience 2*, 127–132, doi:10.1039/NGEO411.

Meehl, G. A., T. F. Stocker, W. D. Collins, P. Friedlingstein, A. T. Gaye, J. M. Gregory, A. Kitoh, R. Knutti, J. M. Murphy, A. Noda, S. C. B. Raper, I. G. Watterson, A. J. Weaver, and Z.-C. Zhao (2007). Global climate projections. In S. Solomon, D. Qin, M. Manning, M. Chen, Z. Marquis, K. Averyt, M. Tignor, and H. Miller (Eds.), *Climate Change 2007: The Physical Science Basis. Contribution of Working Group I to the Fourth Assessment Report of the Intergovernmental Panel on Climate Change*, pp. 747–845. Cambridge, United Kingdom and New York, NY, USA: Cambridge University Press.

Milankovitch, M. (1920). *Théorie Mathématique des Phénomène Thermique Produits par la Radiation Solaire*. Paris: Gauther Villars.

Milankovitch, M. (1930). *Mathematische Klimalehre und Astronomische Theorie der Klimaschwankungen*, Volume I, part A of *Handbuch der Klimatologie*, pp. A1–A176. Berlin: Verlag von Gebrüder Borntraeger.

Milankovitch, M. (1941). *Kanon der Erdbestrahlung und seine Anwendung auf das Eiszeitenproblem*. Belgrade: Acadèmie Royal Serbe.

Myhre, G., E. J. Highwood, K. P. Shine, and F. Stordal (1998). New estimates of radiative forcing due to well mixed greenhouse gases. *Geophysical Research Letters 25*(14), 2715–2718.

North, G. R., J. G. Mengel, and D. A. Short (1983). Simple energy balance model resolving the seasons and the continents: Application to the astronomical theory of the ice ages. *Journal of Geophysical Research 88*(C11), 6576–6586.

Paul, A. and C. Schäfer-Neth (2005). How to combine sparse proxy data and coupled climate models. *Quaternary Science Reviews 23*, 1095–1107, doi:10.1016/j.quascirev.2004.05.010.

Penck, A. and E. Brückner (1901-1909). *Die Alpen im Eiszeitalter*. Leipzig: C. H. Tauchnitz.

Petrović, A. (2002). Insolation and climate. milutin milanković and the mathematical theory of climate changes. Technical report, Ministry for Protection of Natural Resources and Environment of the Republic of Serbia in collaboration with Serbian Society of History of Science.

Rayner, P. J., R. Giering, T. Kaminski, R. Ménard, R. Todling, and C. M. Trudinger (2000). Exercises. In P. Kasibhatla, M. Heimann, P. Rayner, N. Mahowald, R. G. Prinn, and D. E. Hartley (Eds.), *Inverse Methods in Glonal Biogeochemical Cycles*, Volume 114 of *Geophysical Monograph Series*, pp. 81–106. Washington, DC: AGU.

Rougier, J. (2008). Comment on article by sansó et al. *Bayesian Analysis 3*(1), 45–56.

Sarnthein, M., R. Gersonde, S. Niebler, U. Pflaumann, R. Spielhagen, J. Thiede, G. Wefer, and M. Weinelt (2003). Overview of Glacial Atlantic Ocean Mapping (GLAMAP 2000). *Paleoceanography 18*, doi:10.1029/2002PA00769.

Schäfer-Neth, C. and A. Paul (2004). The Atlantic Ocean at the Last Glacial Maximum: 1. Objective mapping of the GLAMAP sea-surface conditions. In G. Wefer, S. Mulitza, and V. Ratmeyer (Eds.), *The South Atlantic in the Late Quaternary: Reconstruction of Material Budgets and Current Systems*, pp. 531–548. Berlin, Heidelberg: Springer-Verlag.

Schneider von Deimling, T., H. Held, A. Ganopolski, and S. Rahmstorf (2006). Climate sensitivity estimated from ensemble simulations of glacial climate. *Climate Dynamics 27*, 149–163, doi:10.1007/s00382–006–0126–8.

Thacker, W. (1989). The role of the hessian matrix in fitting models to measurements. *Journal of Geophysical Research 94*, 6177–6196.

Wessel, P. and W. H. F. Smith (1998). New, improved version of generic mapping tools released. *EOS Transactions of the American Geophysical Union 79*, 579.

Winguth, A. M. E., D. Archer, E. Maier-Reimer, and U. Mikolajewicz (2000). Paleonutrient data analysis of the glacial Atlantic using an adjoint ocean general circulation model. In P. Kasibhatla, M. Heimann, P. Rayner, N. Mahowald, R. G. Prinn, and D. E. Hartley (Eds.), *Inverse Methods in Global Biogeochemical Cycles*, Volume 114 of *Geophysical Monograph Series*, pp. 171–183. Washington, DC: AGU.

Wunsch, C. (1996). *The Ocean Circulation Inverse Problem*. New York: Cambridge University Press.

# 7 Figures

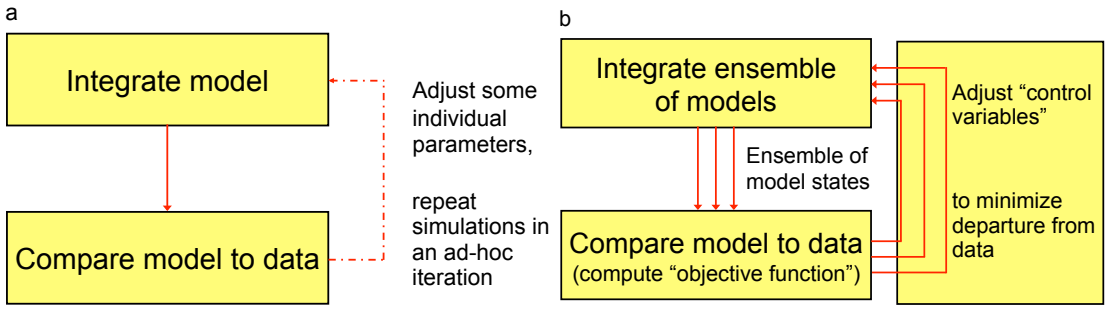


Figure 1: Schematic diagrams for (a) the traditional forward method, (b) statistical inverse methods.

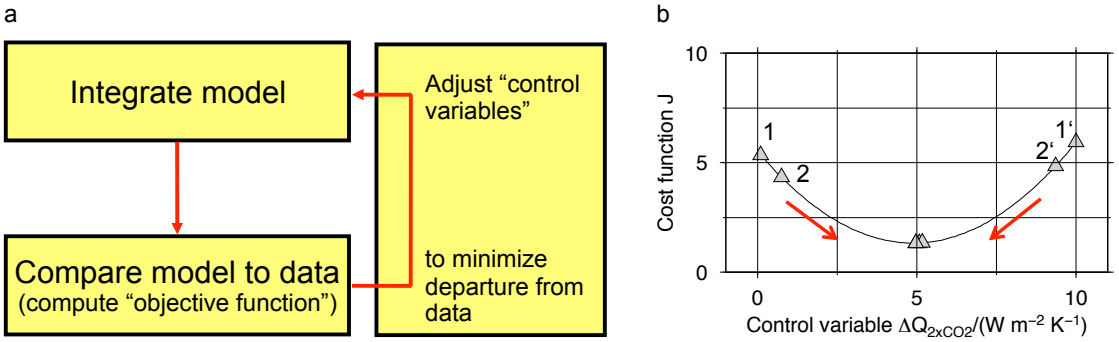


Figure 2: Schematic diagrams for (a) the assimilation of paleoclimate data by the adjoint method, (b) the approach of the minimum of the cost function in Experiment LGM1.

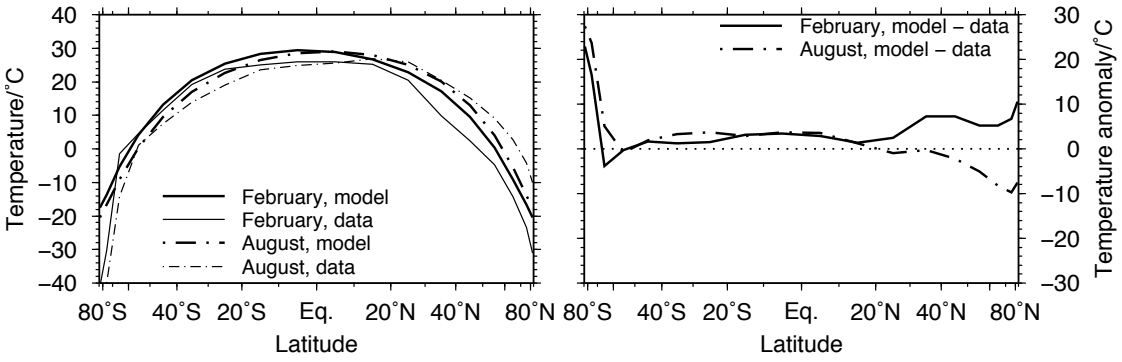


Figure 3: First guess of present-day climate in Experiment PD0. Left: Simulated and observed surface air temperature for February and August. Right: Differences between model and data for February and August.

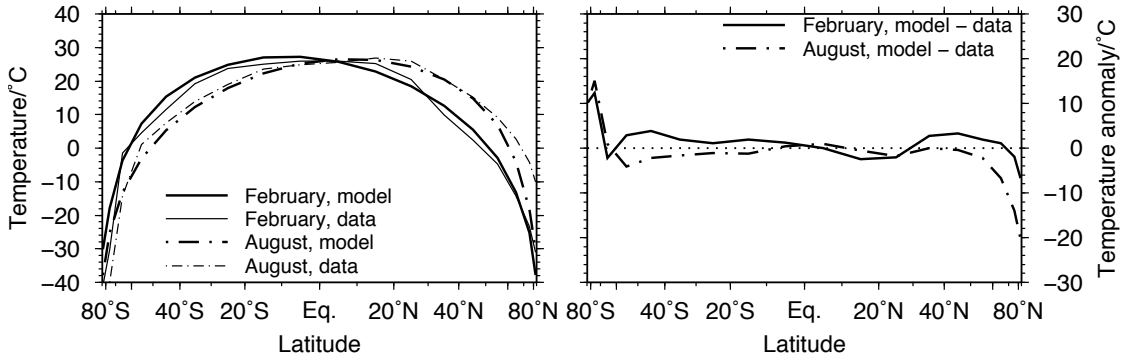


Figure 4: Fit to present-day climate in Experiment PD1 (control variables: diffusion and outgoing longwave radiation parameters). Left: Simulated and observed surface air temperature for February and August. Right: Differences between model and data for February and August.

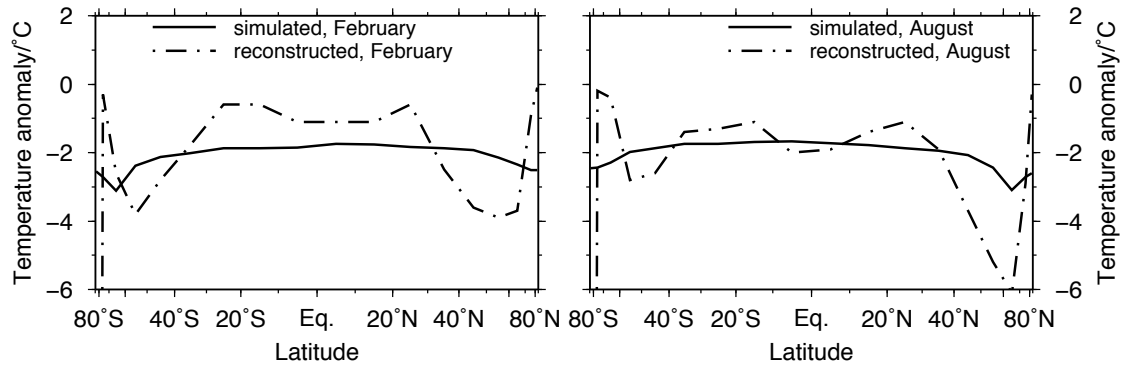


Figure 5: Fit to LGM anomaly in Experiment LGM1 (control variable: $CO_2$ sensitivity). Simulated and reconstructed SST anomaly for (left) February and (right) August.

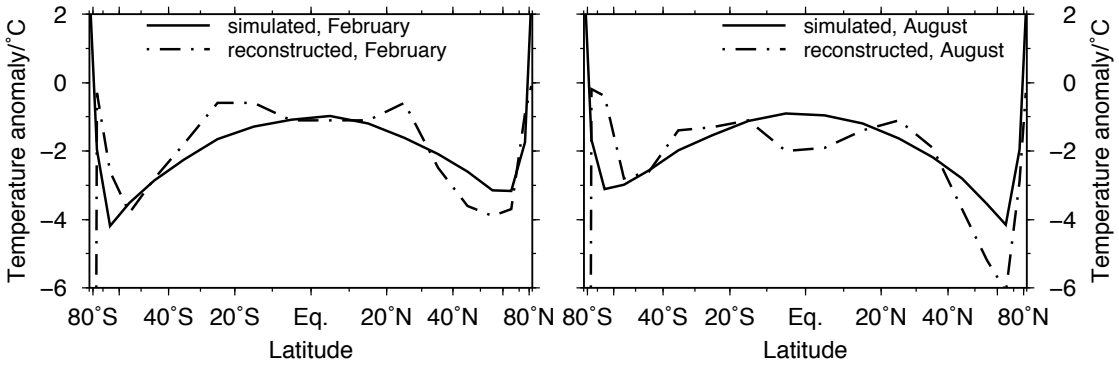


Figure 6: Fit to LGM anomaly in Experiment LGM2 (control variables: diffusion parameters and $CO_2$ sensitivity). Simulated and reconstructed SST anomaly for (left) February and (right) August.

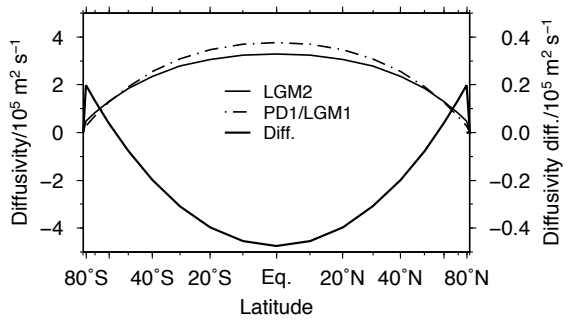


Figure 7: Diffusivity in Experiments PD1/LGM1 and LGM2.

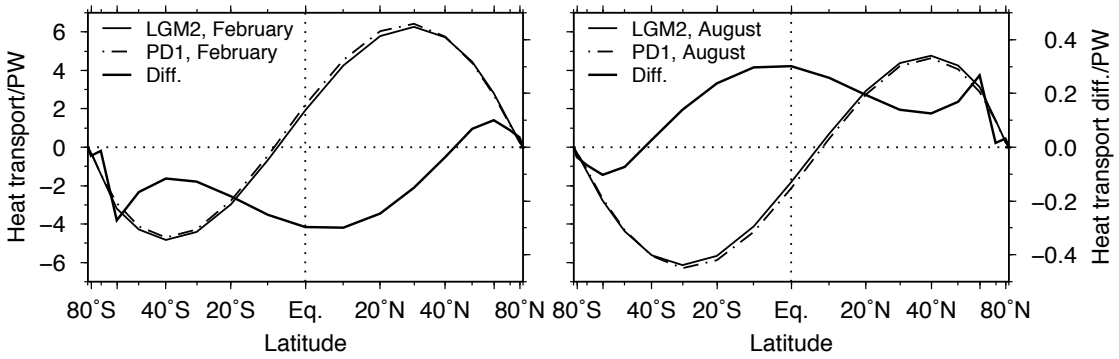


Figure 8: Meridional heat transport in Experiments PD1 and LGM2 for (left) February and (right) August.